Separation Science and Technology

ISSN: 0149-6395 (Print) 1520-5754 (Online) Journal homepage: https://www.tandfonline.com/loi/lsst20

Evaluation and characterization of Pd-Ag composite membrane fabricated by surfactant induced electroless plating (SIEP) for hydrogen separation

M. M. Rahman, M. S. Islam, M. A. Rahman, H. Tun, V. Deshmane, T. Hossain & S. Ilias

To cite this article: M. M. Rahman, M. S. Islam, M. A. Rahman, H. Tun, V. Deshmane, T. Hossain & S. Ilias (2019): Evaluation and characterization of Pd-Ag composite membrane fabricated by surfactant induced electroless plating (SIEP) for hydrogen separation, Separation Science and Technology, DOI: 10.1080/01496395.2019.1576734

To link to this article: https://doi.org/10.1080/01496395.2019.1576734

SEPARATION SCIENCE AND TECHNOLOGY
https://doi.org/10.1080/01496395.2019.1576734

Taylor & Francis
Taylor & Francis Group

Evaluation and characterization of Pd-Ag composite membrane fabricated by surfactant induced electroless plating (SIEP) for hydrogen separation

M. M. Rahman, M. S. Islam, M. A. Rahman, H. Tun, V. Deshmane, T. Hossain, and S. Ilias

Department of Chemical, Biological and Bioengineering North Carolina Agricultural and Technical State University, Greensboro, NC, USA

ABSTRACT

Dense Pd-Ag/MPSS composite membranes were fabricated on macroporous stainless steel substrate (MPSS) by novel surfactant induced electroless plating (SIEP) process. SIEP was effective in synthesizing dense and thinner Pd-Ag films on MPSS with shorter deposition time in presence of cationic DTAB. SIEP membranes showed 3–8 times higher H_2 permeance compared to that of conventional EP membranes. The SEM, XRD, and EDS studies confirmed the formation of Pd-Ag alloy and no diffusion of MPSS substrate metal components into the Pd-Ag film. The Pd-Ag membrane (15 μm thickness) was tested for long-term stability under thermal cycling (623–723-623 K) up to 42 days.

ARTICLE HISTORY
Received 2 November 2018
Accepted 28 January 2019

KEYWORDS
Pd-Ag membrane; thermal stability; H_2 separation; H_2/N_2 selectivity; SIEP

Introduction

Hydrogen is not only one of the most important commodity chemicals in the industry but also a promising clean alternative fuel which can be used both in moving and stationary applications comprising of fuel cells. However, since most of the current hydrogen is produced from the fossil sources which adds significant amount CO_2 in the environment, it negates the advantage of H_2 as a clean alternative fuel.[1] Renewable hydrogen with closed carbon cycle can be produced in abundant quantities using syngas from biomass gasification followed by the water-gas-shift reactions (WGSR): $(\text{Biomass}+O_2+ H_2O \rightarrow CO + CO_2+\text{otherspecies})$ and $(CO+ H_2O \rightarrow CO_2+H_2)$.[2–4] However, the higher capital equipment cost is the bottleneck issue of this process. In the current technology, syngas goes through different stages, primarily high-temperature WGS reaction, low-temperature WGS reaction, and pressure swing adsorption (PSA) involving cooling and heating in-between stages.[5] This significantly increases equipment cost with added energy loss. Furthermore, the lower discharge pressure of the PSA system necessitates a costly compression step for purified gas storage and transportation.[5] Developing H_2 selective membrane systems that can combine the WGS reactions, with no intermittent cooling, and H_2/CO_2 separation at higher temperature and pressure, provides a sustainable and more economical solution.[6] Although, Pd-based membranes with palladium films supported on porous substrates have shown promising results, they have not yet reached a commercial stage due to some technical issues such as long-term permeance, stability, and selectivity.[7] One of the critical issues associated with pure Pd membranes is the hydrogen embrittlement. Pd hydride has two phases; α-phase dominates in low hydrogen concentration and β-phase dominates in high hydrogen concentration. Phase transition is one of the important characteristics of Pd-H phase diagram which occurs in hydrogen concentration below the critical temperature and pressure of 298°C and 20 psi, respectively. Both these phases have identical pure Pd face-centered cubic (FCC) lattice and only differ in their lattice constants. Thus, consecutive hydrogen adsorption/desorption cycles below the critical point causes grain defects and complete loss of hydrogen selectivity. Alloying of Pd with other metals such as Ag, Au, and Cu have shown to not only improve the stability of the membrane but also significantly increase the H_2 permeability.[8] For example, Pd-Ag alloy with 23%Ag demonstrated to have 1.7 times higher permeability compared to pure Pd membrane at 350°C and 2 MPa.[9,10]

Various techniques have been explored to fabricate Pd-Ag alloy membranes with improved long-term stability in the literature.[11–14] Among the different methods, electroless plating (EP) for thin film deposition is

CONTACT S. Ilias ilias@ncat.edu Department of Chemical, Biological and BioengineeringNorth Carolina Agricultural and Technical State University, Greensboro, NC 27411, USA

Color versions of one or more of the figures in the article can be found online at www.tandfonline.com/lsst.
Supplemental data for this article can be accessed here.

regarded as the most promising. In EP, oxidation-reduction reactions between Pd/Ag complex and hydrazine (reducing agent) result in metallic deposition of Pd °/Ag° in a microporous solid surface.[15–17] The formed N_2 and NH_3 gas bubbles in these reactions tend to adhere to the solid–liquid inter-phase, which hinders the deposition of Pd/Ag on the surface resulting a non-uniform film deposition with poor control on Pd/Ag grain sizes. Our research group showed the use of cationic surfactant (DTAB) in EP process to fabricate defect-free Pd film on MPSS substrate.[18] The new surfactant induced EP (SIEP) proved to be an effective method of film fabrication with excellent control in metal deposition rate, grain formation, and agglomeration.[18–20]

In this study, SIEP technique is employed to sequentially deposit Pd and Ag films on MPSS substrate to fabricate defect-free thin Pd-Ag alloy film. The microstructural characterization and H_2-permselectivity of the fabricated Pd-Ag alloy films are discussed in detail. The Pd-Ag membrane fabricated by SIEP method was tested for long-term (42 days) hydrogen permeation measurements at temperatures cycled between 623 and 723 K. The SEM analysis was also done to characterize the membrane after long-term performance test.

Experimental

Material & methods

All materials used were of analytical grade and used without further purification. Isopropanol and ammonium hydroxide (28%) were purchased from Fisher Scientific (New Jersey, USA). Tin chloride dihydrate (98%), tetraamminepalladium (II) chloride monohydrate (≥ 99.99%), dodecyltrimethylammonium bromide (DTAB) (90%), hydrazine solution (1.0 M in tetrahydrofuran), and hydrochloric acid (37%) were procured from Sigma Aldrich (Missouri, USA). Silver nitrate (≥ 99.9%), and palladium (II) chloride (99.9%) were obtained from Alfa Aesar (Massachusetts, USA). Ethylenediaminetetraacetic acid and disodium salt (≥ 99%) were obtained from Acros Organics, New Jersey, USA. The water used at all stages of the experiments was purified using a Mill-Q Advantage A10 with Elix 5 system obtained from Millipore Corporation (Bedford, MA, USA). Macroporous stainless steel (MPSS) discs with 0.062 inch in thickness, 1 inch in diameter, and average pore size 0.2 μm (specifications from supplier – Mott Metallurgical Corporation, Farmington, CT) were used as a substrate for Pd-Ag membrane.

Membrane preparation

The sensitization and activation solutions were prepared using $SnCl_2$ and $PdCl_2$, respectively, in hydrochloric acid to create nucleation sites for the electroless deposition step. The solution composition, pH, temperature, and time used in these steps are summarized in Table 1. The deposition of Pd and Ag on the Sn/Pd-activated MPSS disc was carried out sequentially in EP bath at a constant temperature of 60°C. The detailed fabrication process is discussed elsewhere.[21–23] The composition and operating conditions of the Pd and Ag EP bath used are also provided in Table 1. For the detailed comparative characterization and performance evaluation between conventional EP (henceforth referred as CEP) and SIEP, DTAB concentration of 4 CMC (critical micelles concentration) was used in both Pd and Ag baths. However, based on some further preliminary studies, two changes were made to fabricate the Pd-Ag/MPSS membrane for long-term stability evaluation studies. First, DTAB concentration of 1 CMC in Ag bath instead of 4 CMC and second, an intermediate oxide layer was introduced on MPSS substrate by heat treating it at 873 K for 12 h in presence of air.

Membrane characterization and testing for H_2-permselectivity

The microstructure of the Pd-Ag/MPSS membrane was analyzed using scanning electron microscopy (SEM), energy dispersive X-ray spectroscopy (EDS), X-ray

Table 1. Chemical composition of sensitization, activation, Pd-bath and Ag-bath solutions.

Chemical composition	Sensitization solution	Activation solution	Pd-bath	Ag-bath
$SnCl_2.2H_2O$	1 g/L	-	-	-
$PdCl_2$	-	0.1 g/L	-	-
HCl	1 mL/L	1 mL/L	-	-
$Pd(NH_3)_4Cl_2.H_2O$	-	-	4 gm/L	-
$AgNO_3$	-	-	-	0.519 gm/L
Na_2EDTA	-	-	40.1 gm/L	40.1 gm/L
NH_4OH	-	-	198 mL/L	198 mL/L
NH_2-NH_2	-	-	5.6 mM	5.6 mM
DTAB	-	-	4 CMC	1 CMC
Operating Parameters				
Temperature	20°C	20°C	60°C	60°C
Time	4–6 min	4–6 min	1 h	1 h
pH	4–5	4–5	10 –11	10 –11

diffraction (XRD), and atomic force microscopy (AFM). The grain sizes were determined using point-to-point measurements from representative SEM images. The statistical distributions were estimated considering a minimum 1000 number of grains in a constant cross-section area. The membrane gas tightness (helium leak test) and H_2 permselectivity studies were carried out on the in-house built diffusivity measurement setup.[19] Permeation measurements were made at four different temperatures between 523 K and 823 K with trans-membrane pressure differential up to 100 psi. Prior to the hydrogen permeation measurement, the flow system was preheated to the required temperature at 15 psig hydrogen environment. The cross-section of the membranes tested for the permeability studies were analyzed across the thickness of Pd-Ag/MPSS to investigate the metal diffusivity from Pd-Ag film to support and vice versa by EDS elemental mapping and line scanning at multiple locations across each cross-section. For long-term stability evaluation, the membrane was tested continuously for 42 days on stream under H_2 environment at 623 K to 723 K. The N_2 flux was measured after every 24 h by switching between hydrogen and nitrogen to check the integrity of the membrane.

Results and discussion

Helium gas-tightness and film thickness analysis of Pd-Ag membranes

Microstructure of Pd-based membranes depends on a number of factors, such as substrate surface roughness and pore sizes, fabrication technique and bath parameters. The use of different reducing agents and their concentrations also affects the reaction kinetics, hence, affect the surface microstructure and grain size distribution to some extent. In this study, a number of Pd-Ag/MPSS membranes have been fabricated by both SIEP and CEP process. In order to elucidate the effect of surfactant on the microstructure of the Pd-Ag films, the composition and the operating parameters of the Pd- and Ag-baths were kept constant (Table 1).

The sequential deposition cycles (1 h each) in Pd and Ag bath were continued to achieve the dense Pd-Ag film. It was observed that while SIEP-fabricated sample required 22 h of deposition, CEP sample took 32 h to obtain He leak tight membrane. The films thickness of SIEP and CEP fabricated Pd-Ag films were measured using both SEM and gravimetric analysis method, which were found to be in good agreement. In gravimetric analysis, we used weight gain of the MPSS substrate due to Pd-Ag deposition to estimate the film thickness. The SIEP Pd-Ag/MPSS membrane has a thinner film thickness (~13 μm) compared to the one prepared by CEP (16.77 μm). This is in agreement with our previous work.[20–22] Significant reduction in dense Pd-Ag film thickness was achieved with the use of surfactant. Helium leak test (Supplemental Information, Figure S1) showed that indeed SIEP is very effective in reducing membrane film thickness. Furthermore, it was also observed that the SIEP Pd-Ag films (13 μm) fabricated in the present work are substantially thicker than that of pure Pd film (8.5 μm) prepared using the same method in our earlier work (Supplemental information, Figure S1).[18,21,24] This result is expected due to the considerably different deposition kinetics for Pd and Ag. Since Ag is difficult to deposit on a freshly activated substrate surface, Ag particles deposit on the top of Pd particles in a sequential deposition process. As a result, Ag particles tend to deposit on or around the Pd hills rather than depositing uniformly in the valleys.[21] These fabrication differences along with the interaction with the dimensionally different Pd particles size make the surface rough. This behavior of Ag takes more cycles of deposition to make leak proof Pd-Ag composite membrane resulting in thicker films than the Pd membranes.

Microstructure analysis of Pd-Ag/MPSS membranes

To investigate the particle size, surface roughness and grain boundary diffusion in detail, the SEM images were taken at magnifications of 5, 10, 20, and 40 K as shown in Fig. 1. From the images, it can be inferred that two different particle sizes are dominating the grain sizes and the subsequent agglomeration. Higher magnification SEM images (Fig. 1(c–d)) show the presence of two different-sized particles having two different mean grain sizes. These high magnification images also indicate that there is a similar grain boundary diffusion just beneath the top particle layer. Since fabrication of Pd-Ag membrane was carried out using the sequential SIEP process that ended with Ag deposition, Ag deposits only on the crest of the hills, which ends up with an apparent increase in roughness of the film. For Pd-Ag film, it has a continuous grain boundaries diffused into one another just beneath the rough top layer (with different particle size). This is the combined effect of the interaction of Pd and Ag particles along with the sequential deposition mechanism. Fig. 2 shows the grain size distribution of Pd and Ag in Pd-Ag membrane fabricated using DTAB at 4 × CMC in SIEP. The particle size distribution of Pd and Ag shows two sharp peaks between 0.4 and 1.8 μm. The existence of the two peaks indicates the presence of two separate processes of Pd and Ag deposition in a sequential

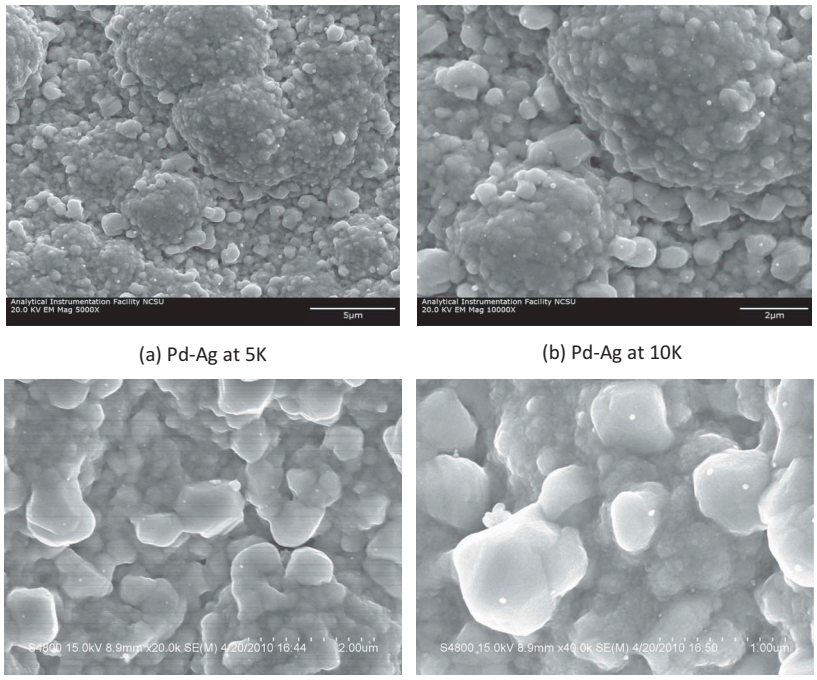

(a) Pd-Ag at 5K (b) Pd-Ag at 10K

(c) Pd-Ag at 20K (d) Pd-Ag at 40K

Figure 1. SEM images of surfactant activated Pd-Ag film showing the surface fabricated by SIEP.

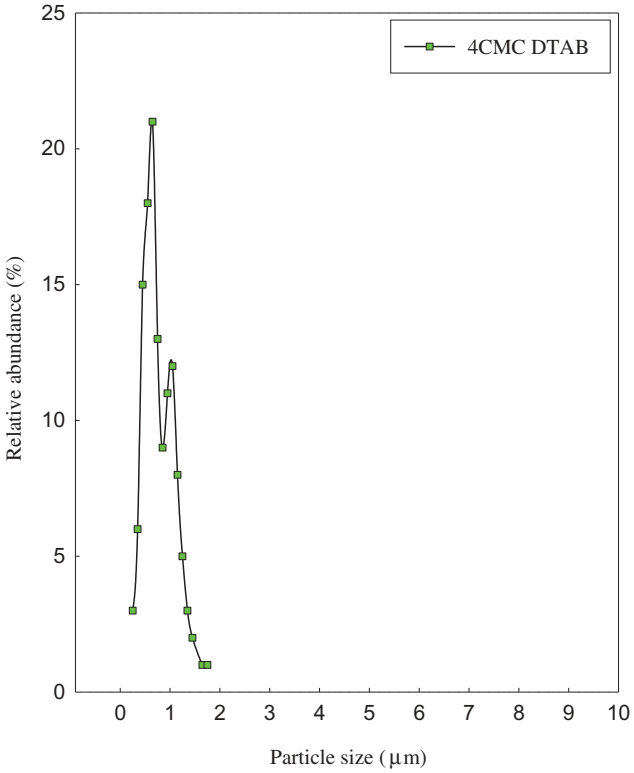

Figure 2. Pd and Ag grain size distribution observed in Pd-Ag membrane fabricated by SIEP process with 4CMC DTAB.

fabrication technique. Both peaks indicated the existence of two different mean size particles, which is consistence with the SEM images presented in Fig. 1.

In a sequential deposition cycle of Pd and Ag while fabricating Pd-Ag membrane, the cycle ends with Ag deposition. The presence of Pd particles in the earlier steps in a cycle, act as a deposition site and accelerate the Ag deposition. To control the metal composition of Ag in Pd-Ag film, it is required to control depositing Pd and Ag in a depositing cycle. Both Pd and Ag have to be deposited before the surface gets deactivated. That actually leaves some unused nucleation sites. Thus, Pd and Ag particles do not get enough particle aggregation into the grain to grow to its normal dimension.

Effect of heat treatment on microstructures

Upon fabrication, Pd-Ag/MPSS membranes were heat-treated in a gas tight diffusion cell for 18 h at 773 K under H_2 environment at 1 atmospheric pressure. The temperature was chosen based on Tamman temperature of Pd, Ag, and substrate metal constituents. Tamman temperature for Pd and Ag are 913 K and 618 K, respectively. For MPSS substrate, it is 823–833 K (Fe: 905 K, Cr: 1090 K & Ni: 905 K). To minimize Fe and other support metal diffusion into the Pd-Ag film, a temperature of 773 K was chosen which is in between Ag and MPSS Tamman temperature. This annealing temperature eventually gave us a film, which was almost free from substrate constituent metals. Surface morphology of a representative Pd-Ag film at pre- and post-annealing conditions is shown in Fig. 3. It is observed

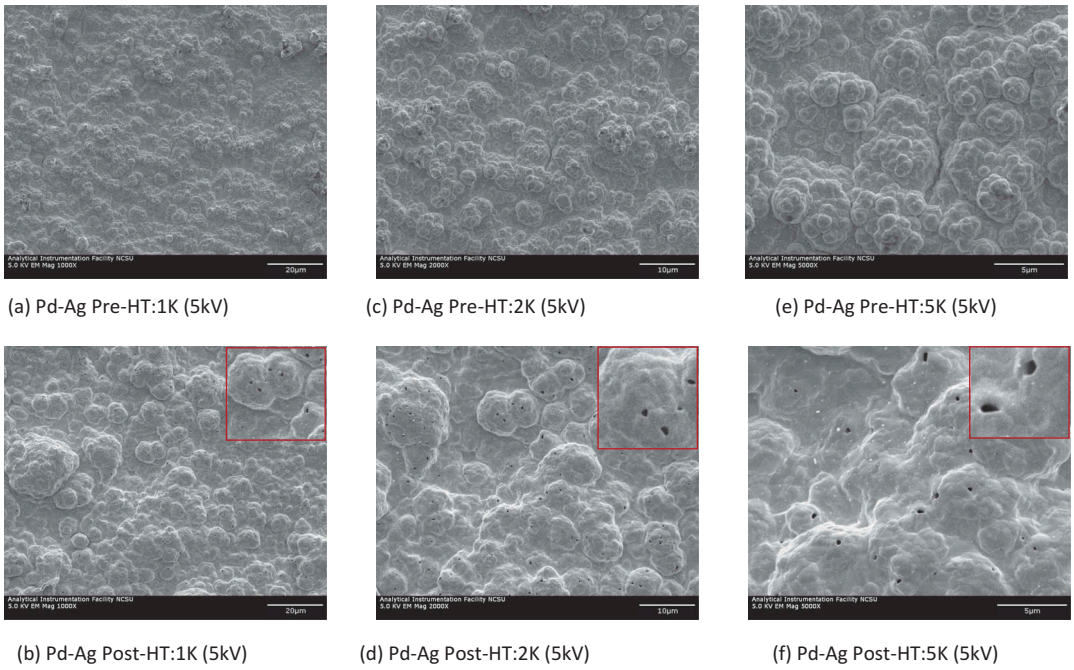

(a) Pd-Ag Pre-HT:1K (5kV) (c) Pd-Ag Pre-HT:2K (5kV) (e) Pd-Ag Pre-HT:5K (5kV)

(b) Pd-Ag Post-HT:1K (5kV) (d) Pd-Ag Post-HT:2K (5kV) (f) Pd-Ag Post-HT:5K (5kV)

Figure 3. SEM images of top surface of Pd-Ag membranes fabricated by SIEP method a pre- and post-HT (heat treatment) conditions at different resolution showing grain agglomeration.

from the SEM images that the smaller grains agglomerated into forming larger grains with recognizable boundaries disappearing after annealing. During the heat treatment of the Pd-Ag film, Ag particles diffused into the Pd layers forming homogeneous alloys of larger clusters. As stated earlier, DTAB is hydrophobic in nature and aligning them around gas-liquid interfaces result in forming various cylindrical and spherical cage-like structures.[18,20,25] Surfactant also tends to form meta-stable structure in the solid-liquid interfaces that helps finer grain formation and subsequent coarsening of the grain. Tiny holes with diameter in the range of 150 to 300 nm were observed upon heat treatment. It is believed that the interstitial spaces might form during the sequential deposition and drying steps. Apart from interstitial spaces, a minute oxidation of the metal might occur during the 2 h drying step. Heat treatment under H_2 environment might drive out that oxygen and other impurities away from the film layers. Occupying the inter-granular spaces in the layers may occur via re-orientation of the crystals. The metals from the top are used up in filling the empty spaces. While cooling starts after heat treatment, recrystallization occurs and diffusion ceases. As a result, these tiny holes are believed to be created on the surface. However, the dense nature of the Pd-Ag films suggests that these holes are only on the top surface and are not penetrated deep in the film. The surface topography was examined with AFM and presented in Fig. 4 for Pd-Ag/MPSS surface. The surface roughness of the Pd-Ag/MPSS was observed to be 2.229 μm, and the surface is largely agglomerated. The cage-like structure in Pd-Ag/MPSS surface is hard to recognize. This may be because of the interaction of different size of particles and different deposition mechanism of the Pd and Ag metals.

Quantitative and qualitative surface elemental analysis was carried out by EDS and XRD, respectively. Typical EDS pattern of Pd-Ag film fabricated using SIEP method is presented in Fig. 5. It shows the intense peaks for Pd and Ag. In the EDS spectrum, it is difficult to distinguish Pd and Ag peaks.[21] However, quantitative EDS elemental analysis of Pd-Ag film shows 24% Ag as presented in Fig. 5. The target metal content was 23% suggesting controlled fabrication of Pd-Ag/MPSS membrane by SIEP technique. As Pd and Ag are placed next to each other in the periodic table, both metals give sharp peak nearly at the same place. An escape peak for Pd at approximately 1.5 KeV X-ray energy is always observed when Pd is involved in the analysis. However, no peaks for any impurities were observed in the EDS spectrum. The EDS pattern demonstrates a representative membrane of target composition. This also implies that the use of surfactant DTAB in the EP solution bath does not introduce any impurities in the membrane film.

In Fig. 6, three XRD patterns (before annealing, after 10 h of annealing and after 18 h of annealing) are shown for Pd-Ag membrane. The XRD pattern for 10 h of annealed film indicates that the alloying of the Pd-Ag

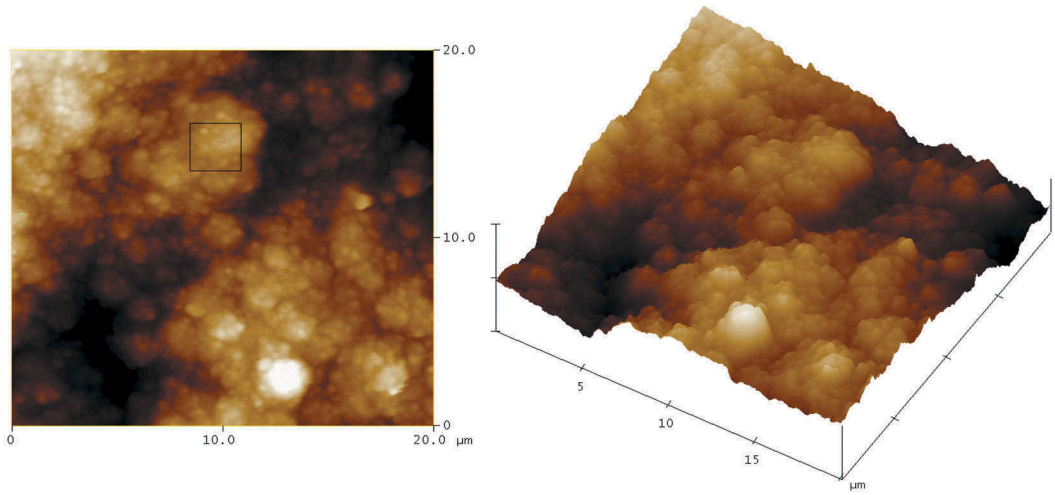

Figure 4. AFM images of solid Pd-Ag surface aggregation onto typical MPSS surface with DTAB.

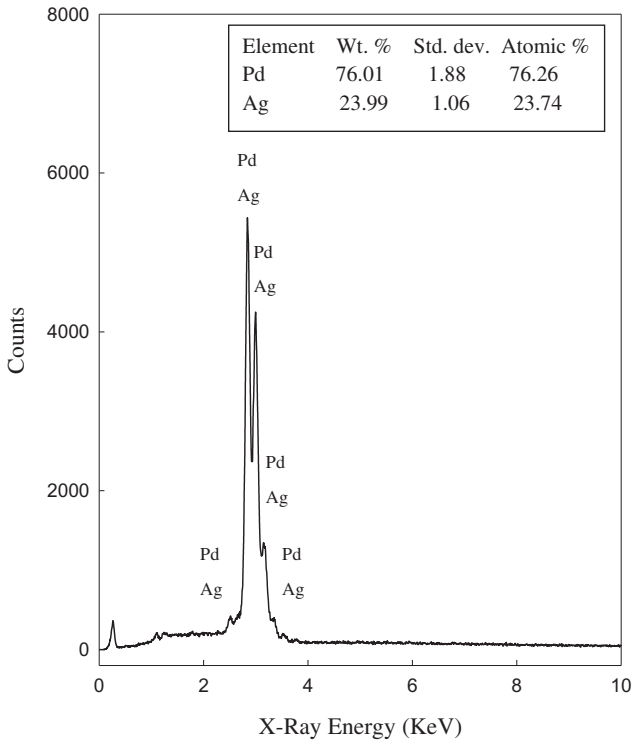

Figure 5. Typical EDS spectrum for Pd-Ag membrane shows the polycrystalline deposition of Pd and Ag particles.

layer is not complete (Fig. 6(b)). Indeed, Pd and Ag peaks shift into the middle and shoulders appeared at the characteristics planes (111), (200), and (220). These shifts of peaks and shoulder formation indicate the co-existence of pure Pd and Ag phases with a Pd-rich Pd-Ag alloy phase.[26,27] After annealing in the same condition for a total of 18 h, a single-phase FCC Pd-Ag alloy is observed at the characteristics planes (Fig. 6(c)). However, the reflection peaks for single-phase FCC Pd-Ag alloy is found in between pure Pd and Ag peaks at 2θ of 39.925, 46.434, and 67.767 for (111), (200), and (220) planes, respectively. Table 2 lists the 2θ and d-spacing values corresponding to the three major reflection peaks (111), (200) and (220). Using Brag's law, the lattice parameter was calculated and was found to be 3.98 Å, which was 4.08 Å for pure FCC Ag. Evidently, this is an indication that the observed increase in the Ag cluster size was associated with the lattice expansion of the Ag metal. These results are in good qualitative agreement with the literature which indicates an annealing temperature of 773 K or above is required to get a homogeneous alloy.[28] It was important to note that, no reflection peaks were observed for any of the substrate support metal (Fe, Cr, Ni & Mn/Mo) in the XRD.

Pd-Ag/MPSS membrane cross-section analysis

A detailed study of Pd-Ag/MPSS membrane cross-section by SEM-EDS analysis was carried out to understand the behavior of metal deposition deep inside the pores. The pores in MPSS substrate are interconnected and tortuous in nature. As an example, in Fig. 7(a), six locations across a depth of 50 µm for Pd and Ag were probed. Metal deposition was found in the pore walls deep inside from the substrate-film interphase. The Pd and Ag metal contents in these pores are shown in Fig. 7(b) by a bar graph. The Ag metal was found to be up to about 50 µm depth inside the pores. However, as expected it decreased across the depth. To further elucidate the metal depositions, Pd-Ag film cross-section at different locations was examined by EDS line-scanning as shown in Fig. 8. As the EDS probe approaches the interface from the far side of the substrate, Pd and Ag peaks jump to their maximum and Fe, Cr, and Ni peaks drop sharply. To understand the relative amount of each metal in the Pd-Ag film, EDS

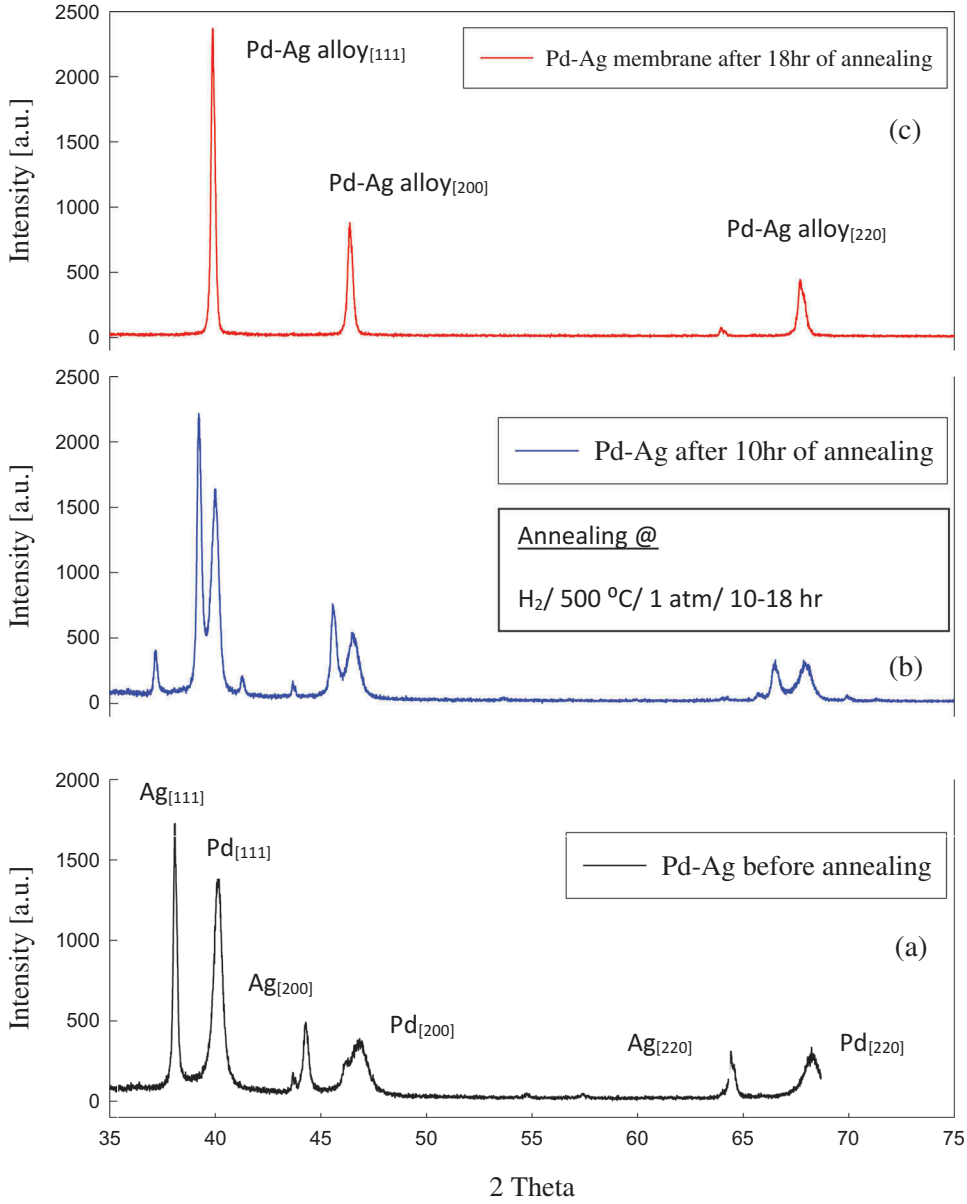

Figure 6. Effect of heat treatment on XRD pattern of Pd-Ag membrane fabricated by SIEP process.

Table 2. Comparison of high angle XRD reflection peaks of Pd- and Pd-Ag-film fabricated by SIEP process.

	Bravais lattice	Pd (Pre annealed)	Ag (Pre annealed)	Pd-Ag (Post annealed)
2-theta	111	40.119	38.115	39.925
	200	46.664	44.299	46.434
	220	68.128	64.443	67.767
d-spacing	111	2.2457	2.3591	2.2562
	200	1.9449	2.0431	1.9540
	220	1.3752	1.4446	1.3816
Lattice parameter, a		3.8898	4.0862	3.9800
Lattice structure		FCC	FCC	FCC

elemental analysis was done on the substrate. The composition of the substrate was found to be 68.73, 16.38, 11.38, 2.52, and 0.79% by weight for Fe, Cr, Ni, Mo, and other trace metals, respectively. Based on the X-ray counts on the line scanning, Ag content in the film was found to be 20.5% which is little lower than the target (24% Ag). A repeated rise and fall of the X-ray counts are observed representing the sequential deposition. The oscillation of X-ray counts is prominent for Ag as the Ag content is low in each deposition cycle. Being the minor constituent, Ni

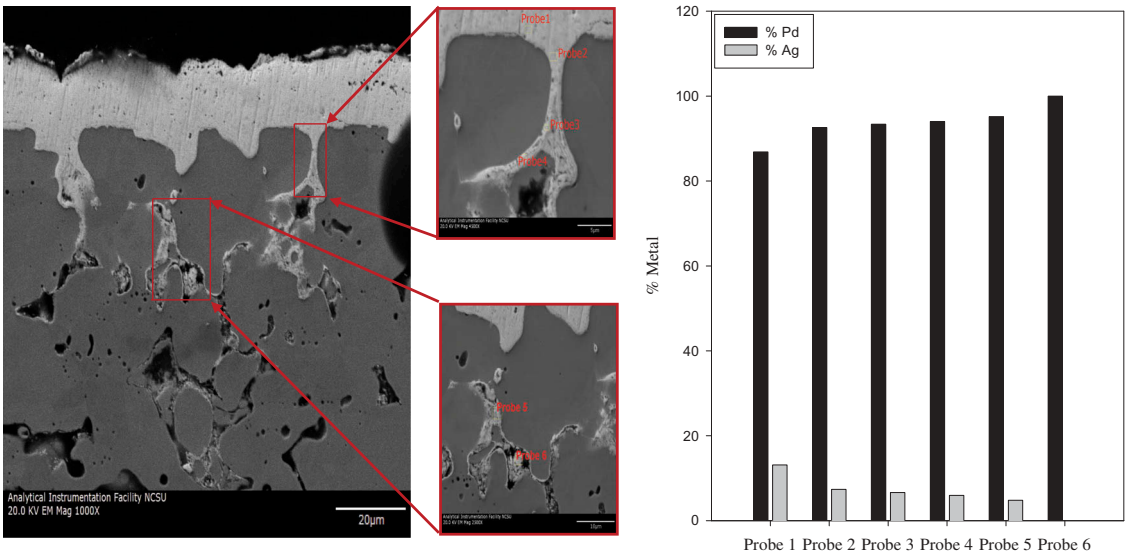

(a) Location of pores for EDS analysis

(b) Metal distribution in pores

Figure 7. SEM images of Pg-Ag film from Pd-Ag membrane cross-section: (a) showing the locations of EDS for metal deposition behavior analysis; (b) Metal (Pd and Ag) distribution during deposition in the pores starting from the pore mouth to the very deep inside (From Probe 1 →Probe 6).

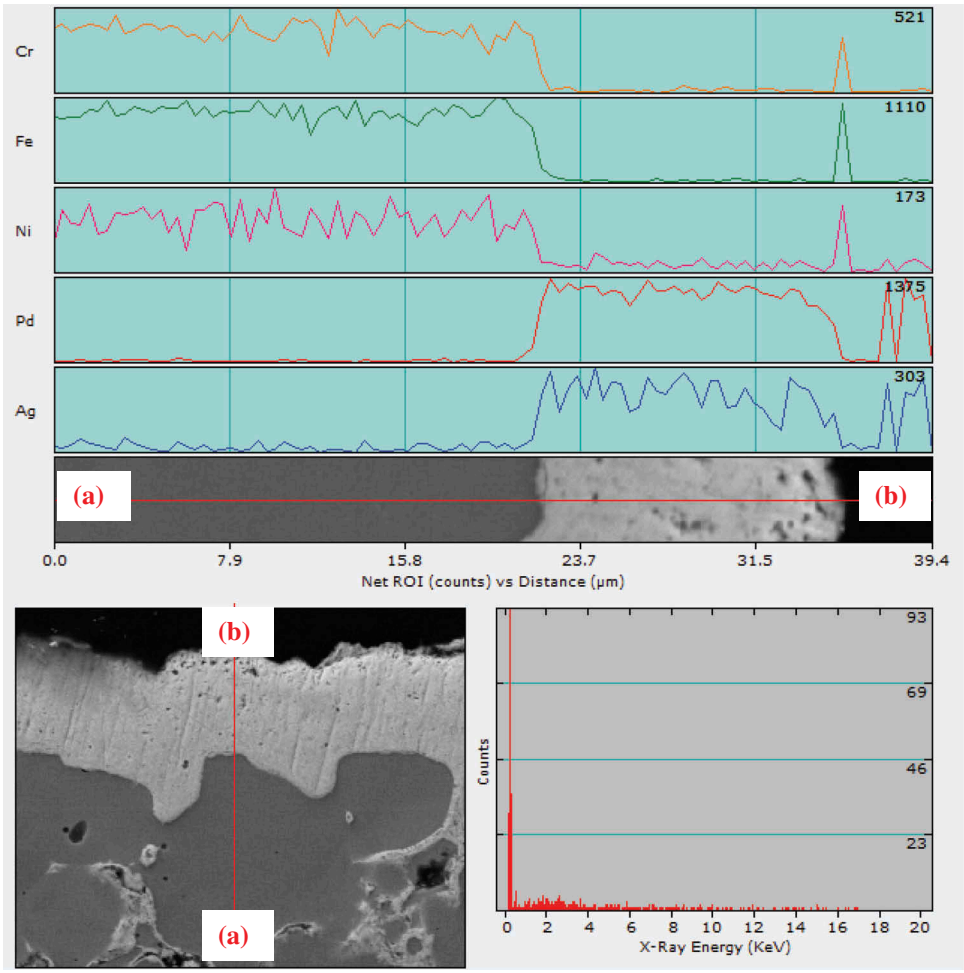

Figure 8. EDS line scanning of Pd-Ag-film cross section [Scanning length 40 μm, scanning direction from (a) → (b)] Ag in Pd-Ag membrane fabricated by SIEP showing the metal distribution in the Pd film and substrate.

has the background effect and oscillates more as confirmed by EDS mapping. However, sharp peaks for Fe, Cr, and Ni (sharp trough for Pd and Ag) at the end of Pd-Ag film are observed. This could be the response from the fine stainless steel particles, which could have been doped in the film or in the resin where the sample was mounted for scanning. It is to be noted that during the sample preparation after cutting, membrane pieces are mounted in the resin and then the resin is cured. The top part is polished with sand paper to expose the membrane cross-section from the resin. As the Pd-Ag-alloy film and polymer matrix are soft, some stainless steel particle from the substrate might get separated and are doped into the film.

EDS mapping was carried out for the membrane cross-section to examine the metal diffusion (Supplemental Information, Figure S2). An infinitesimally small amount of Fe, Cr, and Ni diffusion into the film were observed as expected. As the Tamman temperature for Ag is much lower than Pd (Pd_{Tamman} = 913 K and Ag_{Tamman} = 618 K), heat treatment at 773 K for 18 h under H_2 environment results in relatively higher diffusion of Ag into the substrate compared to that of Pd as shown in Figure S2c. Substrate constituent Fe, Cr, and Ni were found entirely in the substrate. Only few dots for Fe, Cr, and Ni were found in the film. Hence, from EDS mapping, presence of Cr and Fe can be ignored in the film. Post heat treatment, XRD analysis also confirms negligible amount of substrate constituent elements migration into the film at annealing condition.

H_2-permselectivity studies of Pd-Ag membranes

Pd-Ag/MPSS membranes fabricated by the SIEP and CEP processes were tested for gas-tightness and hydrogen perm-selectivity in our permeability measurement set up. The thickness of the Pd-Ag film on MPSS support was found to be about 13 μm as determined by both SEM and weight gain method. When diffusion is not only the rate-limiting step, the hydrogen flux through dense Pd-film is given by Sieverts-type expression as:

$$N_H = \frac{Q_H}{t}\left(P_f^n - P_p^n\right) \quad (1)$$

where Q_H is the hydrogen permeability (a product of solubility and diffusivity), t is the membrane thickness, and $P_f$and P_p are the partial pressures of hydrogen on feed and permeate sides, respectively. The empirical exponent n in Eq. (1) is usually evaluated by non-linear regression. Eq. (1) becomes the Sieverts law when diffusion through the bulk metal is rate-limiting step and the hydrogen concentration into the metal is proportional to the solubility coefficient and square root (n = 0.5) of the hydrogen pressure in the gas phase.[29,30]

Pd-Ag/MPSS membranes fabricated by SIEP and CEP methods were tested for hydrogen flux in the temperature range of 523 to 823 K to evaluate the transport mechanism. The measured data as a function of pressure difference $(P_f - P_p)$ at 523, 623, 723, and 823 K are presented in Fig. 9. The lines drawn in the Fig. 9 are non-linear least-square fit with a power index, n = 0.85 for Pd-Ag/MPSS (SIEP) and 0.8 for Pd-Ag/MPSS (CEP). These values are slightly higher than Sieverts law index. The flux data showed that with increasing temperature, hydrogen flux increased for a given transmembrane pressure. The hydrogen flux also increased with increase in pressure difference across the membrane. More notably, SIEP fabricated Pd-Ag/MPSS membranes showed 3 to 8 times higher H_2 permeance compared to the CEP membrane depending upon the temperature and transmembrane pressure conditions. For example, at 723 K, SIEP, and CEP Pd-Ag/MPSS membranes showed the H_2 flux of 0.80 and 0.18 mol/m^{2}s, respectively. H_2 flux of a membrane for a set of temperature and trans-membrane pressure depends on film thickness, microstructure, and composition of the film. By using surfactant, top surface microstructure of the film can be replicated closely. Still, it is very difficult to replicate the exact film thickness and metal composition of the film for any two membranes. H_2 flux in Fig. 9 represents the flux of Pd-Ag membrane (SIEP) of thickness 12.54 μm and Pd-Ag membrane (CEP) of thickness 16.7 μm. Metal compositions are kept close for both these membranes. A reduction of 25% thickness will enhance the flux significantly but doubling the flux may be attributed to the nanocrystalline microstructure of the deposited film and 23% Ag alloying. Fig. 10 shows the hydrogen-to-nitrogen selectivity results of the same set of membranes. The maximum hydrogen to nitrogen selectivity for Pd-Ag/MPSS membrane at 823 K was found to be 233 and 349 for SIEP and CEP membranes, respectively. Introducing a top Pd-Ag layer after heat treatment, improvement of the selectivity for membranes fabricated by SIEP is possible. But this has a negative impact of losing hydrogen flux considerably.

For Pd-alloy membrane, the pressure exponential factor, n, is typically 0.5 at low pressure but a value of n greater than 0.5 may result when surface processes influence the permeation rate.[31,32] The hydrogen

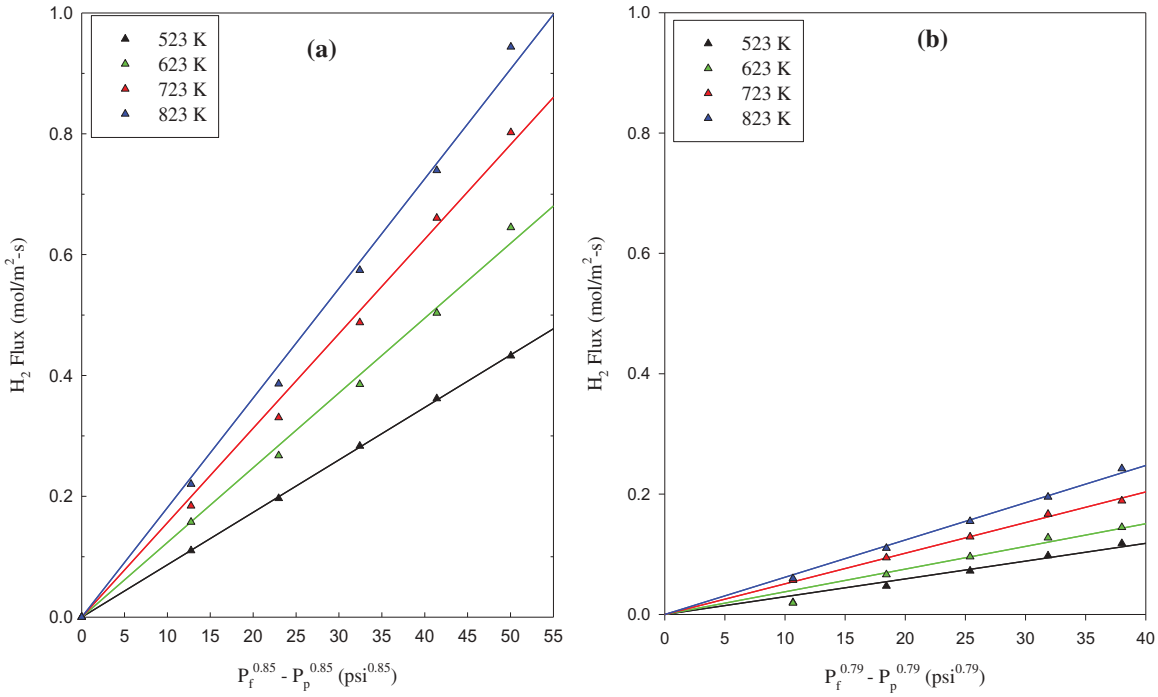

Figure 9. Hydrogen flux at different temperatures in Pd-Ag-MPSS membrane fabricated by (a) SIEP and (b) CEP.

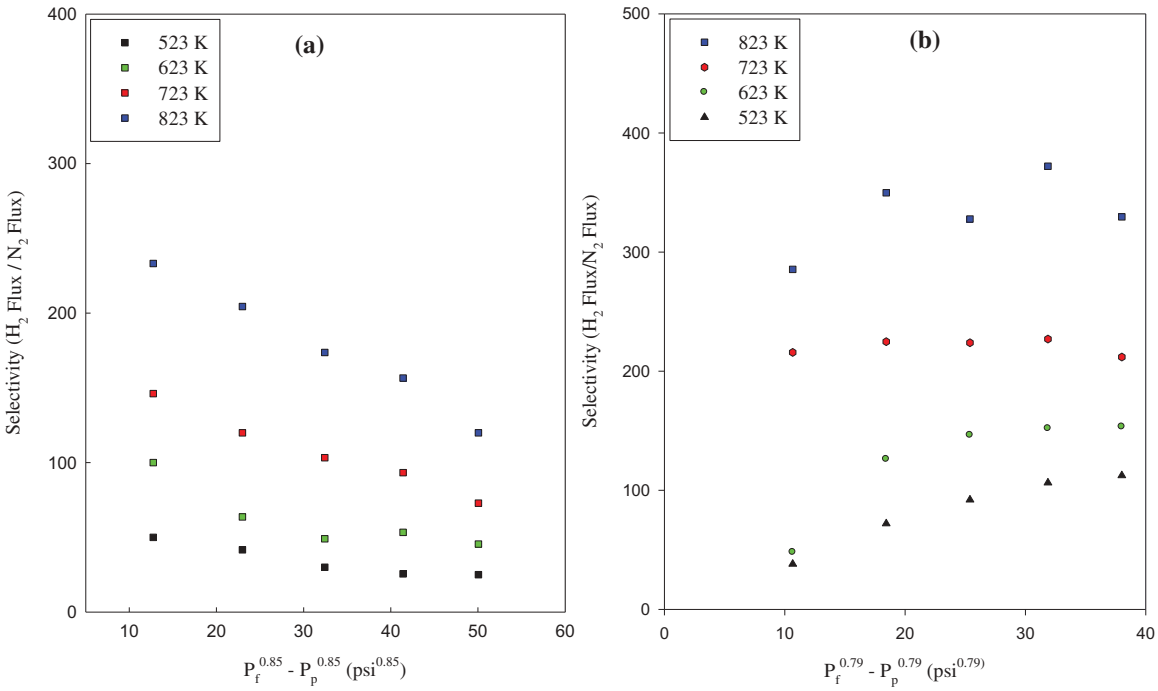

Figure 10. Hydrogen to nitrogen selectivity at different temperatures in Pd-Ag-MPSS membrane fabricated by (a) SIEP and (b) CEP.

diffusivity may become dependent on concentration of dissolved hydrogen and that may contribute to n values greater than 0.5.[33] Leakage of hydrogen through defects in the metal film or membrane seals may also increase the value of n. Further, small resistance of the MPSS membrane support may also slightly increase the value of n. The deviation in the observed flux data from the idealized Sieverts' law may be attributed to some of these contributing factors. From gas-tightness experiment, we are inclined to conclude that Pd-Ag/MPSS membrane (13 μm Pd-Ag film thickness) fabricated by DTAB-induced SIEP is very much defect-free. But, heat treatment produces pinholes which actually reduces the effective

thickness of the perm-selective film. This might make hydrogen dissociation and adsorption a rate-limiting step. Alternatively, it could result in an increased pressure exponent at high pressure.

The computed permeability coefficients (Q_H)at four temperatures are shown in Figure S3 as Arrhenius plot$(Q_H \text{vs} 1/T)$. It gives an excellent fit of the data to Arrhenius equation:

$$Q_H = Q_{Ho} \exp(-E/RT) \quad (2)$$

where $Q_{Ho}$is the reference permeance, E is the activation energy, T is the absolute temperature, and R is the universal gas constant. The activation energy for Pd-Ag film determined was 8.85 KJ/mol, which is lower than the reported values in the literature. For Pd-Ag membrane, an activation energy of 23 KJ/mol was reported for 0.3 μm Pd-Ag film on ceramic support.[34,35] For the latter case, since the hydrogen-to-nitrogen selectivity was reported as low as 5.7, it is difficult to assess the membrane quality. Furthermore, hydrogen fluxes were studied in the temperature range of 373–523 K. Reduction of the particle size in the film thickness and fabrication of an agglomerated microstructure may have resulted in lower activation energy for the membranes. Nanocrystalline palladium has almost 10 times higher diffusivity than conventional polycrystalline Pd. In small nanocrystalline metal, at least 20 to 50% of its atom located in the grain boundaries act as a network for faster diffusion.[36]

Long-term thermal stability test

The Pd-Ag/MPSS membrane fabricated by SIEP process was examined for long-term performance test in H_2 and N_2 environment as shown in Fig. 11. During the fabrication of this membrane, 4 × CMC and 1 × CMC of DTAB surfactants were used in Pd and Ag baths, respectively. According to gravimetric method, the thickness of this membrane was 15.08 μm. For the first 25 days, the membrane was subjected to several thermal cycling at 623–723–623 K and at 15 psig transmembrane pressure. After 25 days of continuous operation, the transmembrane pressure was increased to 20 psig and thermal performance test was continued. During this continuous operation, the membrane showed a good stability with no N_2 gas leakage through the membrane. For the first 25 days, the hydrogen flux at 623 K and 723 K were 0.032 mol/m^2·s and 0.040 mol/m^2·s, respectively. Then, at 20 psig, the hydrogen fluxes were increased to 0.057 mol/m^2·s and 0.069 mol/m^2·s at 623 K and 723 K, respectively. After 42 days of continuous operation, slight N_2 leakage of 0.003 mol/m^2·s was detected at 623 K and 20 psig with H_2 to N_2 selectivity of 23. This indicates that up to 42 days there were no pinholes in the Pd-Ag/MPSS membrane. It was assumed that some layers of the Pd-Ag membrane surface were peeled off during the continuous operation. These peeled off spots of the membrane surface became pinholes after a long run.[37]

After the long-term stability test, Pd-Ag/MPSS membrane was characterized by SEM analysis to observe the microstructure of Pd-Ag alloy film. As discussed earlier in Fig. 3, upon annealing at 773 K for 18 h under hydrogen environment, small pinholes were observed. However, these pinholes were not connected to the substrate surface and no helium leakage was found. After long-term thermal stability performance, similar pinholes were also detected in SEM images. Although over the performance period, the membrane showed the

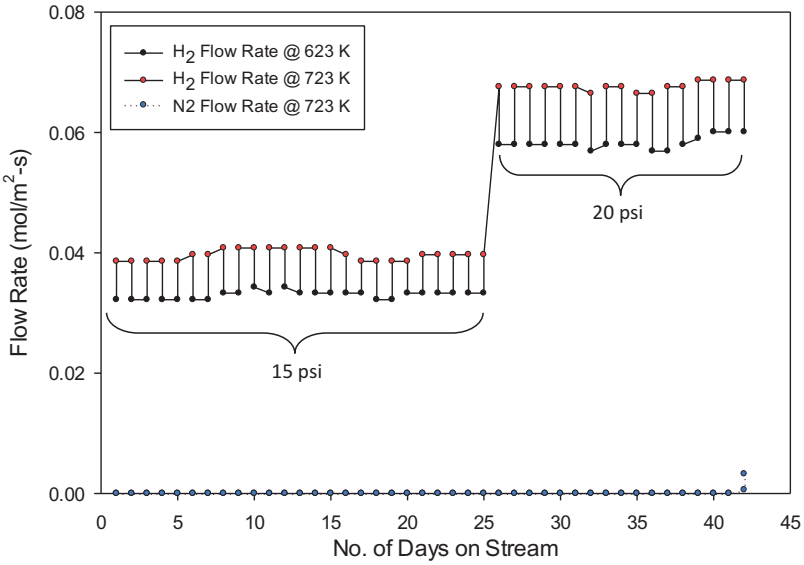

Figure 11. Long-term H_2 and N_2 flux of the Pd-Ag membrane fabricated by SIEP process.

infinite H_2/N_2 selectivity, after 42 days of prolonged operation, small amount of N_2 flow was detected and these pinholes may be the main source of the N_2 leakage.

Figure 12 shows the SEM images of the Pd-Ag/MPSS composite membrane at different magnification after 42 days of continuous operation at 623–723 K and 15–20 psi transmembrane pressure. During the prolonged operation, the Pd-Ag film seems to be peeled off from the surface and some spots of the peeled off area passed through the film and became pinholes. Sintering could also have played an important role in the formation and growth of leaks, since the membrane was operated at 623–723 K which was about 0.2 to 0.4 times the melting temperature of Pd. From SEM images, it was observed that the top surface of the film took a shape of cauliflower. Similar observations were also made in the earlier long-term stability tests with Pd/MPSS membrane.[21]

Furthermore, stored excess energy (such as stress, surface energy in grain boundaries) of the materials can be released in many ways such as sintering, dislocation, and crystallization. These mechanisms are diffusion-controlled mechanism. Diffusion becomes fast when the activation energy for nucleation is achieved and then structural changes occur. At temperature close to Tamman temperature, Pd and Ag atoms acquire sufficient mobility. This may affect microstructure of the film, which may result leak formation.

Conclusions

Defect-free, dense and thin Pd-Ag/MPSS membranes were fabricated using surfactant DTAB in EP bath. Surfactant in SIEP effectively removes N_2 and NH_3 gases from the substrate surface and increases the deposition rate. These two factors help in uniform Pd and Ag deposition resulting in significantly reduced Pd-Ag film thickness with a shorter deposition time. In a sequential deposition, surfactant is capable of configuring a film with grain size distribution of

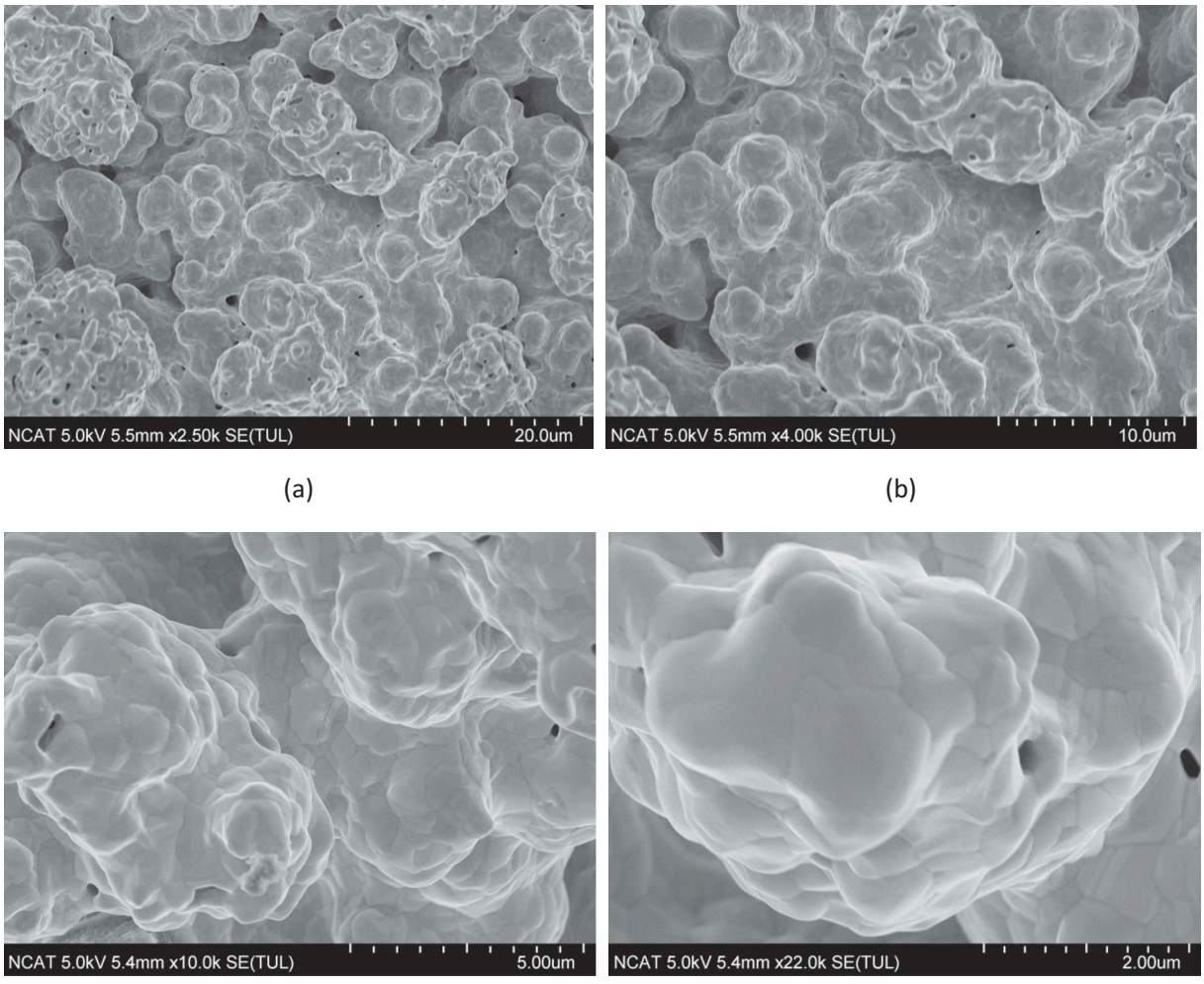

Figure 12. Top surface SEM images of long-term stability tested Pd-Ag composite membrane at different magnification (a) 2.5 k, (b) 4.0 k, (c) 10 k and (d) 22 k.

0.8 to 1.2 μm for Pd-Ag/MPSS membrane. Moreover, surfactant successfully protects dendrite formation and the grains are found to be largely agglomerated. Smaller particle size and grain agglomeration combined with the reduction of film thickness hugely enhanced the H_2 permeability. This could also be attributed to the lower activation energy determined for Pd-Ag film (8.85 KJ/mol) compared to the reported values in the literature. The stability studied up to 42 days showed Pd-Ag/MPSS membranes to be promising for long-term operations.

Acknowledgments

This research was funded by the U.S. Department of Energy – National Energy Technology Laboratory (Award No. DE-FG 08-NT000143). Analytical support from the Center for Advanced Materials and Smart Structures (CAMSS) of North Carolina A&T State University gratefully acknowledged. We gratefully acknowledge the financial support received from the National Science Foundation (NSF) (Grant No: HRD-124215) to reanalyze the previous data and write this manuscript.

Funding

This work was supported by the National Science Foundation (NSF) [HRD-124215];Office of Fossil Energy [DE-FG08-NT 000143].

References

[1] Silva, J.M.; Soria, M.; Madeira, L.M. (2015) Challenges and strategies for optimization of glycerol steam reforming process. *Renewable and Sustainable Energy Reviews*, 42: 1187–1213. doi:10.1016/j.rser.2014.10.084

[2] Department of Energy. (2016) *Quadrennial Technology Review-an Assessment of Energy Technology and Research Opportunities*; Department of Energy: Washington DC.

[3] Department of Energy. (2015) *Bioenergy Technology Office- Multi-Year Program Plan*; Department of Energy: Washington DC.

[4] Borgognoni, F.; Tosti, S.; Vadrucci, M.; Santucci, A. (2011) Pure hydrogen production in a Pd–ag multi-membranes module by methane steam reforming. *International Journal of Hydrogen Energy*, 36: 7550–7558. doi:10.1016/j.ijhydene.2011.03.120

[5] Smart, S.; Lin, C.; Ding, L.; Thambimuthu, K.; Da Costa, J.D. (2010) Ceramic membranes for gas processing in coal gasification. *Energy & Environmental Science*, 3: 268–278. doi:10.1039/b924327e

[6] Wang, H.; Dong, X.; Lin, Y.S. (2015) Membrane reactors for hydrogen production from coal. *Membrane Reactors for Energy Applications and Basic Chemical Production*, Basile, A.; Di Paola, L.; Hai, F.; Piemonte, V. editors; Woodhead Publishing: Cambridge, UK, pp. 145–186.

[7] Pomerantz, N.; Ma, Y.H. (2011) Novel method for producing high H_2 permeability Pd membranes with a thin layer of the sulfur tolerant Pd/Cu FCC phase. *Journal of Membrane Science*, 370: 97–108. doi:10.1016/j.memsci.2010.12.045

[8] Gallucci, F.; Fernandez, E.; Corengia, P.; van Sint Annaland, M. (2013) Recent advances on membranes and membrane reactors for hydrogen production. *Chemical Engineering Science*, 92: 40–66. doi:10.1016/j.ces.2013.01.008

[9] Conde, J.J.; Maroño, M.; Sánchez-Hervás, J.M. (2017) Pd-based membranes for hydrogen separation: review of alloying elements and their influence on membrane properties. *Separation & Purification Reviews*, 46: 152–177. doi:10.1080/15422119.2016.1212379

[10] Basile, A.; Iulianelli, A.; Longo, T.; Liguori, S.; De Faloco, M. (2011) Pd-based selective membrane state of the art. *Membrane Reactors for Hydrogen Production Processes*, De Faloco, M.; Marrelli, L.; Iaquaniello, G. editors; Springer-Verlag: London, UK, pp. 21–55.

[11] Gryaznov, V. (2000) Metal containing membranes for the production of ultrapure hydrogen and the recovery of hydrogen isotopes. *Separation & Purification Reviews*, 29: 171–187. doi:10.1081/SPM-100100008

[12] Pereira, A.I.; Pérez, P.; Rodrigues, S.; Mendes, A.; Madeira, L.; Tavares, C. (2015) Deposition of Pd–Ag thin film membranes on ceramic supports for hydrogen purification/separation. *Materials Research Bulletin*, 61: 528–533. doi:10.1016/j.materresbull.2014.10.055

[13] Okazaki, J.; Ikeda, T.; Tanaka, D.P.; Sato, K.; Suzuki, T.M.; Mizukami, F. (2011) An investigation of thermal stability of thin palladium–silver alloy membranes for high temperature hydrogen separation. *Journal of Membrane Science*, 366: 212–219. doi:10.1016/j.memsci.2010.10.011

[14] Fernandez, E.; Medrano, J.A.; Melendez, J.; Parco, M.; Viviente, J.L.; van Sint Annaland, M.;, *et al.* (2016) Preparation and characterization of metallic supported thin Pd–Ag membranes for hydrogen separation. *Chemical Engineering Journal*, 305: 182–190. doi:10.1016/j.cej.2015.09.119

[15] Bhandari, R.; Ma, Y.H. (2009) Pd–Ag membrane synthesis: the electroless and electro-plating conditions and their effect on the deposits morphology. *Journal of Membrane Science*, 334: 50–63. doi:10.1016/j.memsci.2009.02.014

[16] Shu, J.; Grandjean, B.; Ghali, E.; Kaliaguine, S. (1993) Simultaneous deposition of Pd and Ag on porous stainless steel by electroless plating. *Journal of Membrane Science*, 77: 181–195. doi:10.1016/0376-7388(93)85068-8

[17] Cheng, Y.S.; Yeung, K.L. (2001) Effects of electroless plating chemistry on the synthesis of palladium membranes. *Journal of Membrane Science*, 182: 195–203. doi:10.1016/S0376-7388(00)00563-9

[18] Ilias, S.; Islam, M.A. Methods of preparing thin films by electroless plating. *United States Patent 8,298,620*. 2012.

[19] Islam, M.A.; Ilias, S. (2010) Characterization of Pd-composite membrane fabricated by surfactant induced electroless plating (SIEP): effect of grain size on hydrogen permeability. *Separation Science and Technology*, 45: 1886–1893. doi:10.1080/01496395.2010.493823

[20] Islam, M.S.; Rahman, M.M.; Ilias, S. (2012) Characterization of Pd–Cu membranes fabricated by surfactant induced electroless plating (SIEP) for hydrogen

separation. *International Journal of Hydrogen Energy*, 37: 3477–3490. doi:10.1016/j.ijhydene.2011.11.024

[21] Islam, S.Z.; Deshmane, V.G.; Ilias, S. (2016) Thermal stability study of Pd-composite membrane fabricated by surfactant induced electroless plating (SIEP). *Separation Science and Technology*, 51: 1176–1188. doi:10.1080/01496395.2015.1109661

[22] Islam, M.A. (2008) The development of improved electroless plating in fabricating Pd-based membrane and membrane reactor application for hydrogen separation. PhD Dissertation, Energy and Environmental Studies, North Carolina A & T State University: Greensboro.

[23] Rahman, M.M. (2010) Fabrication of Pd and Pd-Ag membranes by surfactant induced electroless plating (SIEP). MS Thesis, Chemical and Bioengineering, North Carolina A & T State University: Greensboro.

[24] Islam, S.Z. (2012) A study on thermal stability of palladium-composite membrane fabricated by surfactant induced electroless plating (SIEP). MS Thesis, Chemical and Bioengineering, North Carolina A&T State University: Greensboro.

[25] Ayturk, M.E.; Engwall, E.E.; Ma, Y.H. (2007) Microstructure analysis of the intermetallic diffusion-induced alloy phases in composite Pd/Ag/porous stainless steel membranes. *Industrial and Engineering Chemistry Research*, 46: 4295–4306. doi:10.1021/ie061677j

[26] Lin, W.-H.; Chang, H.-F. (2006) AFM, EDS and XRD microstructural characterizations of Pd-Ag/PSS membranes. *Journal of the Chinese Institute of Chemical Engineers*, 37: 239–247.

[27] Mardilovich, P.P.; Ying, S.; Yi Hua, M.; Min-Hon, R. (1998) Defect-free palladium membranes on porous stainless-steel support. *AIChE Journal*, 44: 310–322. doi:10.1002/aic.690440209

[28] Lin, W.-H.; Chang, H.-F. (2005) Characterizations of Pd-Ag membrane prepared by sequential electroless deposition. *Surface and Coatings Technology*, 194: 157–166. doi:10.1016/j.surfcoat.2004.07.089

[29] Vadrucci, M.; Borgognoni, F.; Moriani, A.; Santucci, A.; Tosti, S. (2013) Hydrogen permeation through Pd–Ag membranes: surface effects and Sieverts' law. *International Journal of Hydrogen Energy*, 38: 4144–4152. doi:10.1016/j.ijhydene.2013.01.091

[30] Basile, A.; Campanari, S.; Manzolini, G.; Iulianelli, A.; Longo, T.; Liguori, S. et al. (2011) Methane steam reforming in a Pd–Ag membrane reformer: an experimental study on reaction pressure influence at middle temperature. *International Journal of Hydrogen Energy*, 36: 1531–1539. doi:10.1016/j.ijhydene.2010.10.101

[31] Fahler, S.; Weisheit, M.; Krebs, H.U. (1998) In-situ characterization of laser deposited Fe/Ag multilayers by a combination of time-of-flight, RHEED and resistance measurements. In *Situ Process* Diagnostics *and Intelligent Materials* Processing. *Symposium, 2–5 Dec. 1997*, Warrendale, PA, pp. 139–144.

[32] Fernandez, E.; Coenen, K.; Helmi, A.; Melendez, J.; Zuñiga, J.; Pacheco Tanaka, D.A.;, *et al.* (2015) Preparation and characterization of thin-film Pd–Ag supported membranes for high-temperature applications. *International Journal of Hydrogen Energy*, 40: 13463–13478. doi:10.1016/j.ijhydene.2015.08.050

[33] Huang, T.-C.; Wei, M.-C.; Chen, H.-I. (2002) Preparation of palladium-silver alloy composite membranes for hydrogen permeation. *Chemical Engineering Communications*, 189: 1262–1282. doi:10.1080/00986440213885

[34] Uemiya, S.; Sato, N.; Ando, H.; Kude, Y.; Matsuda, T.; Kikuchi, E. (1991) Separation of hydrogen through palladium thin film supported on a porous glass tube. *Journal of Membrane Science*, 56: 303–313. doi:10.1016/S0376-7388(00)83040-9

[35] Jayaraman, V.; Lin, Y.S. (1995) Synthesis and hydrogen permeation properties of ultrathin palladium-silver alloy membranes. *Journal of Membrane Science*, 104: 251. doi:10.1016/0376-7388(95)00040-J

[36] Jayaraman, V.; Lin, Y.S.; Pakala, M.; Lin, R.Y. (1995) Fabrication of ultrathin metallic membranes on ceramic supports by sputter deposition. *Journal of Membrane Science*, 99: 89. doi:10.1016/0376-7388(94)00212-H

[37] Gleiter, H. (1989) Nanocrystalline materials. *Progress in Materials Science*, 33: 223–315. doi:10.1016/0079-6425(89)90001-7